Journal of Biomolecular NMR, **14:** 1–12, 1999.
KLUWER/ESCOM

Self-consistent ^3J coupling analysis for the joint calibration of Karplus coefficients and evaluation of torsion angles

Jürgen M. Schmidt*, Markus Blümel, Frank Löhr & Heinz Rüterjans**
Institut für Biophysikalische Chemie, Johann Wolfgang Goethe-Universität, Biozentrum N230, Marie-Curie-Strasse 9, D-60439 Frankfurt am Main, Germany

Received 20 October 1998; Accepted 19 January 1999

Key words: cross validation, data redundance, ϕ torsion angle, vicinal coupling constants

Abstract

The concept of self-consistent *J* coupling evaluation exploits redundant structure information inherent in large sets of ^3J coupling constants. Application to the protein *Desulfovibrio vulgaris* flavodoxin demonstrates the simultaneous refinement of torsion-angle values and related Karplus coefficients. The experimental basis includes quantitative coupling constants related to the polypeptide backbone ϕ torsion originating from a variety of heteronuclear 2D and 3D NMR correlation experiments, totalling 124 $^3J(H^N,H^\alpha)$, 129 $^3J(H^N,C')$, 121 $^3J(H^N,C^\beta)$, 128 $^3J(C'_{i-1},H^\alpha_i)$, 121 $^3J(C'_{i-1},C'_i)$, and 122 $^3J(C'_{i-1},C^\beta_i)$. Without prior knowledge from either X-ray crystallography or NMR data, such as NOE distance constraints, accurate ϕ dihedral angles are specified for 122 non-glycine and non-proline residues out of a total of 147 amino acids. Different models of molecular internal mobility are considered. The Karplus coefficients obtained are applicable to the conformational analysis of ϕ torsions in other polypeptides.

Introduction

Modelling of macromolecular structure on the basis of NMR spectroscopy (Wüthrich, 1986; Roberts, 1993) increasingly utilizes ^3J coupling constants that probe the orientation of bond vectors between specified pairs of nuclei. Restriction in torsion angle space as derived from ^3J coupling constants facilitate convergence in protein structure calculation protocols primarily based on distance bounds, such as distance-geometry algorithms (Güntert et al., 1991, 1997) and distance-restrained molecular dynamics simulation (van Gunsteren and Berendsen, 1985; Brünger and Karplus, 1991; Brünger et al., 1998). Modern stable-isotope enrichment techniques involving ^{15}N and/or ^{13}C alleviate the sensitive determination of complete sets of homo- and heteronuclear *J*-coupling constants in biomolecules (Bax et al., 1994; Biamonti et al., 1994; Case et al., 1994; Eberstadt et al., 1995). Torsion angles are then fitted to these sets of NMR structure parameters, usually on a per-residue basis, aimed at retrieving details on conformational restrictions along the polymer chain. As previous investigations pointed out (Blackledge et al., 1993; Schmidt, 1997b), routine model building is deemed to not exhaust the information content in ^3J parameter sets. Characterization of molecular geometry might be improved by a novel self-consistent data evaluation strategy as outlined below.

Provided empirical coefficients are available, ^3J values and angular constraints are interconverted by the well-known Karplus equation (Karplus, 1963):

$$^3J(\theta) = A\cos^2\theta + B\cos\theta + C \qquad (1)$$

θ is the dihedral angle subtended by those three consecutive covalent bonds that connect the coupled nuclei considered, and *A*, *B*, and *C* are the associated empirical coefficients (given in Hz) that depend on

*Present address: Division of Molecular Structure, National Institute for Medical Research, Mill Hill, London NW7 1AA, U.K.
**To whom correspondence should be addressed.
Supplementary material: Table S1, showing the complete set of experimental and back-calculated *J* coupling constants for the rigid-geometry model, can be obtained from the authors.

the nature of these nuclei as well as on their specific chemical environment (Haasnoot et al., 1980, 1981). Much theoretical and experimental effort has been devoted to refine Karplus coefficients for the different types of J couplings relevant to dihedral-angle studies on biomolecules (Bystrov, 1976). Yet, accurate prediction of ^3J coupling constants from given molecular constitution and conformation according to Equation 1 is not satisfactory, the more so as the reverse process of deriving dihedral-angle conformation from a given set of experimental ^3J coupling constants is actually requested.

Transformation of ^3J coupling information into angular constraints is complicated by a number of ambiguities:

1. The intrinsic degeneracy of the Karplus relation in Equation 1 gives rise to multi-valued solutions being resolved only by simultaneous equations constructed from a family of coupling constants the members of which depend differently on the same torsion angle (Mierke and Kessler, 1992; Blümel et al., 1998).
2. Uncertainties in the empirical Karplus coefficients have been shown to delicately affect the interpretation of ^3J values with respect to geometry, in particular if a complex ensemble of conformations underlies the few experimentally accessible coupling constants (Karimi-Nejad et al., 1994).
3. In the context of a rigid molecular model, neglect of dynamic averaging effects on the observed ^3J values (Jardetzki, 1980; Hoch et al. 1985) spoils the straightforward translation between spin-system and conformational parameters.
4. Substituent effects were found to significantly modulate the simple relationship in Equation 1, leading to most intricate generalized Karplus relations like those available for $^3J_{HH}$ in cyclic compounds (Haasnoot et al., 1980, 1981).

Empirical calibration of the angular dependence of ^3J couplings in polypeptides is usually based on relating accurately measured ^3J values to dihedral angles available from high-resolution X-ray diffraction studies (DeMarco et al., 1978a,b; De Marco and Llinás, 1979; Pardi et al., 1984; Ludvigsen et al., 1991; Vuister and Bax, 1993; Hu and Bax, 1997). Such an approach critically premises that molecular average conformations in both solution and crystalline environment are identical and that local angular mobility agrees within narrow margins. Aimed at assimilated experimental conditions of target and reference samples, conformationally constrained model compounds have been studied in solution as to derive proper empirical Karplus coefficients (Fischman et al., 1980). However, other issues are raised as the atomic substituent patterns of non-natural amino-acid building blocks in the design compounds rarely match those in the molecule of interest. With the particular interest in balancing and minimizing the problems (1) through (4) addressed above, the present work focuses on translating ^3J coupling information into accurate angular constraints on the exclusive basis of NMR J-coupling data. At the same time, reliable Karplus coefficients are obtained without taking recourse to X-ray data.

The concept

Owing to the high degree of correlation in J coupling information, torsion-angle geometry is determined by the unique pattern in a sufficient number of J values. For example, the set of the six ^3J couplings associated with the protein backbone torsion ϕ (Figure 1) never can adopt all possible value combinations. In the context of a single rigid ϕ orientation, the six experimental determinants are opposed to a single adjustable dihedral angle, thus giving rise to five degrees of freedom. The true extent of overdetermination is somewhat lower as at least three units of reference J information are consumed per torsion-angle determination (Schmidt, 1997a, b), reflecting the degeneracy intrinsic to the Karplus relationship.

The new strategy proposed exploits redundant structure information inherent in a cumulative set of coupling constants related to identical torsions in all subunits of the biopolymer studied. Redundant J coupling information as gathered from the manifold of, for example, amino acid residues, forms a pool of excess degrees of freedom. Besides delivering dihedral angle values, these data are readily tapped to refine initial estimates of all involved Karplus coefficients (three per coupling type), to detect and characterize angular conformational equilibria, or to assess distortion of ideal bonding geometry and substituent effects. For the following rationalization, all ^3J values belonging to a specified torsion type are arranged into an array. Figure 2 exhibits the data organization of the six three-bond couplings $^3J(H^N,H^\alpha)$, $^3J(H^N,C')$, $^3J(H^N,C^\beta)$, $^3J(C'_{i-1},H^\alpha_i)$, $^3J(C'_{i-1},C'_i)$, and $^3J(C'_{i-1},C^\beta_i)$ related to the ϕ torsion in polypeptides. When back-calculating J coupling constants

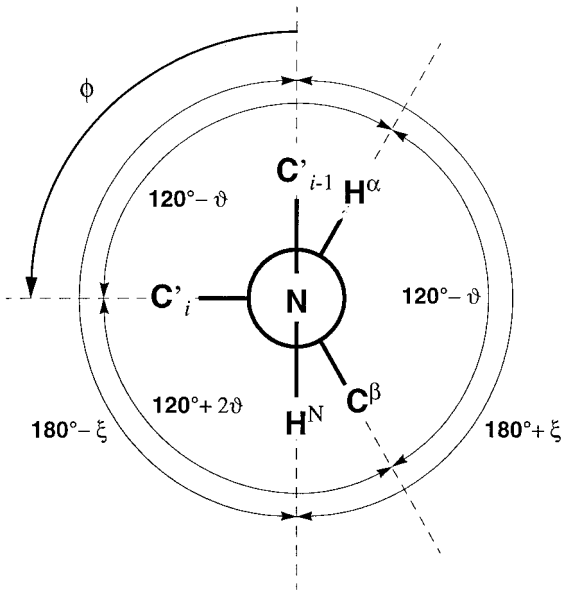

Figure 1. Newman projection of the polypeptide ϕ torsion viewed along the N-C^{α} bond axis. The conformation displayed ($\phi = -90°$) is typical of protein secondary structure. Subscripts i and $i-1$ denote the current and the preceding residue in the polypeptide sequence, respectively. Dihedral angle increments $\xi = \theta(H^{N}\text{–}C^{\alpha}\text{–N–}C'_{i-1}) - 180°$ and $2\vartheta = \theta(C^{\beta}\text{–N–}C^{\alpha}\text{-}C'_{i}) - 120°$ account for possible distortion of ideal planar and tetrahedral bond geometry at N and C^{α} sites, respectively. The definition chosen warrants $\phi = \theta(C'_{i-1}\text{–N–}C^{\alpha}\text{–}C'_{i})$ always.

using Equation 1, data redundance is exploited by realizing that variation of Karplus coefficients and torsion angle parameters affects columns and rows of the J matrix, respectively. Combining 'vertically' and 'horizontally' acting parameter groups, Karplus coefficients and torsion angles, respectively, crucially ties together all constituent J information such that a least-squares regression procedure, termed self-consistent J evaluation, will be driven by the effect of redistributing fit deviations over the complete J array. Firstly, it will be outlined how the basic parameters Karplus coefficients and torsion angles are simultaneously adjusted in order to match back-calculated and experimental coupling constants. In a second stage, the model complexity will be increased as sufficient degrees of freedom are available to study the effect of relaxing various assumptions initially made.

Materials and methods

Sample protein and determination of three-bond coupling constants

Methods are demonstrated on the 147 amino acid electron-transfer protein *Desulfovibrio vulgaris* flavodoxin (16.3 kDa), the biochemical properties of which have been extensively reviewed (Mayhew and Ludwig, 1975; Ghisla and Massey, 1989; Mayhew and Tollin, 1992). Recent crystallographic studies delivered a 1.7 Å resolution model of *D. vulgaris* flavodoxin containing non-covalently bound flavine mononucleotide (FMN) cofactor in the oxidized state (M. Walsh, unpublished; Watt et al., 1991). A preliminary solution structure emerged from a set of 1350 interproton distances obtained from homonuclear and ^{1}H, ^{15}N-heteronuclear NMR spectra (Knauf et al., 1993, 1996). Recently available ^{13}C-enriched protein enabled comprehensive measurements of almost all ^{3}J coupling constants related to the protein backbone torsions ϕ (Löhr and Rüterjans, 1995; Löhr, 1996; Schmidt et al., 1996; Löhr et al., 1997, Blümel et al., 1998). Both the huge amount of experimental J coupling information and the fairly accurate characterization of the protein's global fold render *D. vulgaris* flavodoxin suitable to test the self consistent conversion of ^{3}J coupling information into dihedral-angle constraints.

Isotopically labelled recombinant flavodoxin, both ^{15}N-singly and ^{13}C, ^{15}N-doubly enriched, was prepared according to previous reports (Curley et al., 1991). NMR experiments were carried out at 300 K using protein sample concentrations of 4.5 mM (^{15}N) and 1.4 mM (^{13}C, ^{15}N) in 0.5 ml 10 mM potassium phosphate buffer at pH 7 containing 5% D_2O. NMR spectra were recorded on a Bruker DMX-600 spectrometer equipped with a 5 mm triple-resonance probe and pulsed-field gradient (PFG) accessories, except for $^{3}J(H^{N},C')$ determinations for which an older AMX-600 console and a sample concentration of 2.2 mM were used. The following summarizes the essentials of data collection and evaluation protocols which have been presented elsewhere in detail.

$^{3}J(H^{N},H^{\alpha})$ coupling constants originated from constant-time J-modulated ^{1}H, ^{15}N heteronuclear multiple-quantum coherence (HMQC) spectra in combination with non-linear fitting of the transfer function, taking experimental $^{1}H^{\alpha}$-selective T_1 relaxation times into account (Billeter et al., 1992; Kuboniwa et al., 1994). $^{3}J(H^{N},C')$ coupling constants were

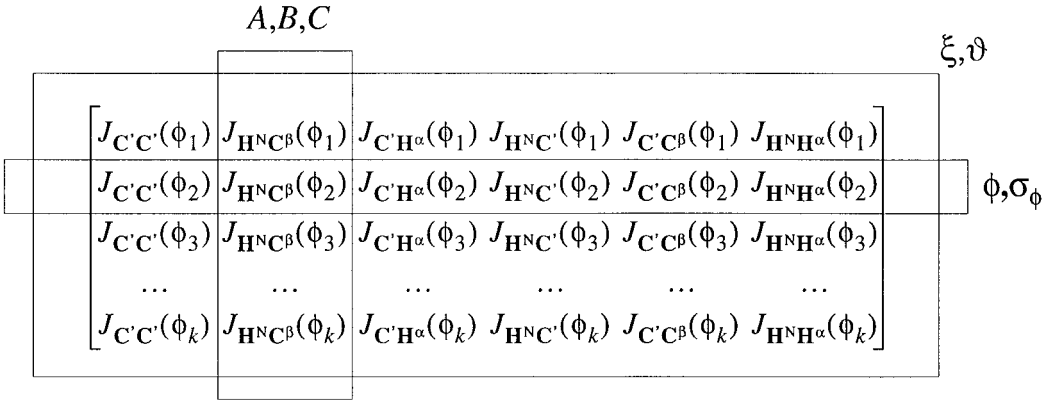

Figure 2. Dependence of back-calculated ^3J coupling constants on model parameters in self-consistent torsion angle calibration. Three groups of adjustables are distinguished: (1) the *J*-coupling type-specific Karplus coefficients affect data columns; (2) the data rows are influenced by residue-specific properties like torsion angles and Gaussian-librational widths; (3) global properties, which are not associated with either a particular *J* coupling type or with a particular residue, such as correction terms accounting for tetrahedral or planar distortion give rise to variation in all entries in the *J* matrix.

obtained using 3D heteronuclear relayed exclusive correlation spectroscopy (E.COSY) combined with 2D multiplet line-shape analysis (Schmidt et al., 1996) and from 3D C′-coupled (H)CANNH spectra (Löhr and Rüterjans, 1995). $^3J(H^N,C^\beta)$ coupling constants resulted from a PFG version of the 3D C^β-coupled (H)CANNH experiment (Löhr and Rüterjans, 1995). $^3J(C'_{i-1},H^\alpha_i)$ coupling constants were measured in 3D H^α-coupled H(N)CA,CO (Löhr et al., 1997) and in a PFG-based 3D C′-coupled (H)NCAHA spectrum (Löhr and Rüterjans, 1995). $^3J(C'_{i-1},C'_i)$ and $^3J(C'_{i-1},C^\beta_i)$ coupling constants resulted from H(N)CA,CO-E.COSY experiments (Löhr et al., 1997) using iterative trace alignment (Schmidt et al., 1995). Coincident chemical-shift ranges of C^α and C^β spins in serine and threonine residues prevented discrimination by selective excitation pulses and prompted additional H^N- and C′-coupled HNCACB experiments (Löhr and Rüterjans, 1999) to determine coupling constants $^3J(H^N,C^\beta)$ and $3J(C'_{i-1},C^\beta_i)$, respectively. In total, 745 quantitative ^3J coupling constants were collected. In case multiple determinations were made due to different experimental approaches, values were averaged provided their error margins were roughly similar.

Model function and implementation

Numerical parameter optimization is considerably facilitated by recasting the torsion-angle dependence of the *J* coupling constant − as Karplus (1963) originally suggested − into a series of (real) Fourier coefficients truncated after the third term,

$$J(\theta) = \sum_{m=0}^{2} C_m \cos(m\theta) = C_0 + C_1\cos(\theta) + C_2\cos(2\theta), \qquad (2)$$

where the identities $A = 2C_2$, $B = C_1$, and $C = C_0 - C_2$ restore the coefficients of the usually applied power series of Equation 1. Physical interpretation of the redefined coefficients remains transparent as C_0 is the mean *J* value obtained upon complete revolution of θ, $(C_2 - C_1)$ is the largest deflection in *J* from the mean, with $2C_1$ being the coupling difference between *trans* and *cis* periplanar orientations of the dihedral angle θ.

As shown in Figure 2 experimental *J* coupling data are deliberately arranged in a matrix J, the size of 122×6 for the ϕ determination in the flavodoxin case, with its elements $J^{\text{expt}}_{k,l}$ made up of the experimental coupling constants of residue *k* and coupling type *l*. The system of linear equations is then given by the short-hand matrix construct J = TC, where the elements in the pseudodiagonal coefficient matrix C are identified with the parameters C_m, $m = 0, 1, 2$ in Equation 2, and T is the matrix of trigonometric cosine operators raised to the series of Fourier components, $T^m_{k,l} = \cos(m\theta_{k,l})$. The dihedral-angle argument includes phase shifts as defined in Table 1, so that $\theta = \phi + l\pi/3$ with $l = 0,...,5$ to conform with the IUPAC/IUB definition (1970) of the heavy-atom torsion ϕ (Figure 1). Perfect trigonal planar and tetrahedral geometries at the backbone nitrogen and C^α atoms, respectively, are assumed. The explicit matrix equation reads:

Table 1. Self-consistent Karplus coefficients for the angular dependence of polypeptide ϕ-related ^3J couplings based on flavodoxin data

Coupling type	Karplus coefficients[a]			Torsion phase increments[b]			
	A (Hz)	B (Hz)	C (Hz)	l	$\Delta\phi$ (deg)	ξ	ϑ
$^3J(H^N,H^\alpha)$	7.90 ± 1.02	-1.05 ± 0.54	0.65 ± 0.58	5	-60	$-\xi$	$-\vartheta$
$^3J(H^N,C'_i)$	4.41 ± 0.81	-1.36 ± 1.03	0.24 ± 0.37	3	± 180	$-\xi$	
$^3J(H^N,C^\beta)$	2.90 ± 0.80	-0.56 ± 0.52	0.18 ± 0.37	1	$+60$	$-\xi$	-2ϑ
$^3J(C'_{i-1},H^\alpha)$	3.76 ± 1.05	-1.63 ± 0.56	0.89 ± 0.60	2	$+120$		$-\vartheta$
$^3J(C'_{i-1},C'_i)$	1.51 ± 0.86	-1.09 ± 1.11	0.52 ± 0.39	0	± 0		
$^3J(C'_{i-1},C^\beta_i)$	2.72 ± 0.80	-0.31 ± 0.52	0.39 ± 0.37	4	-120		-2ϑ

[a]Coefficients given are for use with the equation $^3J(\theta) = A\cos^2\theta + B\cos\theta + C$ where $\theta = \phi + \Delta\phi + \xi + \vartheta$ according to Figure 1. In the basic study $\xi = 0$ and $\vartheta = 0$. The definition chosen warrants that the dihedral angle $\theta(C'_{i-1}\text{–}N\text{–}C^\alpha\text{–}C'_i)$ is always identical to ϕ. Previously established procedures (Schmidt et al., 1996, 1997a, and references cited therein) were applied to obtain $\pm 1\sigma$ confidence boundaries on the Karplus coefficients. Tests were made against the critical Fisher variance ratio $F = 1.137$, given the numbers of observables and adjustables, $n = 705$ and $p = 140$, respectively. Variances σ_m^2 of the Fourier coefficients C_m translate into the usual representation of Karplus parameters according to $\sigma_A^2 = 2\sigma_2^2$, $\sigma_B^2 = \sigma_1^2$ and $\sigma_C^2 = |\sigma_2^2 - \sigma_0^2|$.
[b]Dihedral angle increments $\xi = \theta(H^N\text{–}C^\alpha\text{–}N\text{–}C'_{i-1}) - 180°$ and $2\vartheta = \theta(C^\beta\text{–}N\text{–}C^\alpha\text{–}C'_i) - 120°$ account for possible distortion of ideal planar and tetrahedral bond geometry at N and C^α sites, respectively.

$$\begin{bmatrix} J_{1,1} & J_{1,2} & \ldots & J_{1,l} \\ J_{2,1} & J_{2,2} & \ldots & J_{2,l} \\ J_{3,1} & J_{3,2} & \ldots & J_{3,l} \\ \ldots & \ldots & \ldots & \ldots \\ J_{k,1} & J_{k,2} & \ldots & J_{k,l} \end{bmatrix} =$$

$$\begin{bmatrix} T^0_{1,1} \ldots T^0_{1,l} & T^1_{1,1} \ldots T^1_{1,l} & T^2_{1,1} \ldots T^2_{1,l} \\ T^0_{2,1} \ldots T^0_{2,l} & T^1_{2,1} \ldots T^1_{2,l} & T^2_{2,1} \ldots T^2_{2,l} \\ T^0_{3,1} \ldots T^0_{3,l} & T^1_{3,1} \ldots T^1_{3,l} & T^2_{3,1} \ldots T^2_{3,l} \\ \ldots \ldots \ldots & \ldots \ldots \ldots & \ldots \ldots \ldots \\ T^0_{k,1} \ldots T^0_{k,l} & T^1_{k,1} \ldots T^1_{k,l} & T^2_{k,1} \ldots T^2_{k,l} \end{bmatrix} \begin{bmatrix} C_{0,1} & 0 & \ldots & 0 \\ 0 & C_{0,2} & \ldots & 0 \\ \ldots & \ldots & \ldots & \ldots \\ 0 & 0 & \ldots & C_{0,l} \\ C_{1,1} & 0 & \ldots & 0 \\ 0 & C_{1,2} & \ldots & 0 \\ \ldots & \ldots & \ldots & \ldots \\ 0 & 0 & \ldots & C_{1,l} \\ C_{2,1} & 0 & \ldots & 0 \\ 0 & C_{2,2} & \ldots & 0 \\ \ldots & \ldots & \ldots & \ldots \\ 0 & 0 & \ldots & C_{2,l} \end{bmatrix} \quad (3)$$

When establishing the T matrix, phase shifts $\Delta\phi$ on the heavy-atom torsion ϕ are imposed by exploiting the relationship $\exp\{i(\phi + \Delta\phi)\} = \exp(i\phi)\exp(i\Delta\phi)$ in a complex vector multiplication. Only the real part of the exponential is required for function evaluation, while gradient computation takes advantage of the imaginary component.

Computational protocol

The basic procedure of self-consistent J coupling evaluation relies on the assumption of a single rigid protein conformation. The analysis of the ϕ-related J couplings in flavodoxin allows to adjust 18 Karplus coefficients and 122 torsion angles of non-glycine and non-proline residues exhibiting at least 4 coupling constants each. These 140 independent variables were simultaneously optimized in an iterative manner to minimize the difference between experimental coupling constants J^{expt} and values J^{calc} back-calculated by means of Equation 2. Agreement with experiment was continuously assessed by the normalized residual

$$\epsilon_j^2 = \sum_i^n \sigma_i^{-2}(J_i^{\text{expt}} - J_i^{\text{calc}})^2 = \sum_{k=1}^{122}\sum_{l=0}^{5} \sigma_{k,l}^{-2}[J_{k,l}^{\text{expt}} - C_{0,l} - C_{1,l}\cos(\phi_k + l\pi/3) - C_{2,l}\cos\{2(\phi_k + l\pi/3)\}]^2 \quad (4)$$

where i runs over all n observations. A uniform experimental error in the coupling constants of $\sigma_j = 0.25$ Hz was applied in the self-consistent J-coupling analysis. Qualitatively, the significance of the regression manifests in a small J residual ϵ_J^2 on the order of the number of experimental observables or, more conveniently, in the derived quantity rmsd_J, the rms difference between back-calculated and experimental coupling constants.

At the expense of one additional parameter per residue, local angular mobility is included in the basic model by supplying each torsion angle with a Gaussian probability distribution. Within the frame-

work of a Gaussian libration model, dihedral angles of only those 117 residues were fitted which exhibit at least 5 known coupling constants. The extended variable set comprised additional spread parameters, so that a total of 252 variables were simultaneously optimized. The averaging effect on the Karplus relations is conveniently computed by replacing the Fourier components in Equation 2 by $\langle\cos(m\theta)\rangle = \exp(-m^2\sigma_\theta^2/2)\cos(m\theta)$ reflecting a Gaussian width parameter σ_θ (Brüschweiler and Case, 1994), where the brackets denote ensemble averaging and σ_θ values are given in radians.

Initial Fourier coefficients $C_{0,l}$ and $C_{2,l}$ were set to the means of the experimental J coupling constants averaged for each coupling type l separately, while coefficients $C_{1,l}$ were initialized at -1 Hz. Dihedral angle values ϕ_k were chosen at random from the 2π interval. In the context of Gaussian mobility, the distribution width parameters σ_θ were initialized at 20° using torsion angles and coefficients emerged from the simpler rigid model.

While torsion-angle parameters were freely adjustable, Fourier coefficients were constrained to positive and negative ranges for C_0/C_2 and C_1, respectively, by adding a semi-parabolic penalty $\Delta\epsilon^2_{\text{cons}} = K_{\text{cons}}C^2$ to the residual ϵ^2 defined in Equation 4 that drives the line search. The weighting factor K_{cons} was chosen to represent the number of deviates considered in the residual such as to consume one degree of freedom upon a 1 Hz constraint violation. Gaussian distribution parameters were fitted in the logarithm to avoid the need of constraining their values to physically meaningful positive numbers.

The refinement protocol included a repeatedly restarted least-squares optimization based on the DFP variable-metric method (Davidson, 1959; Fletcher and Powell, 1963), which avoids direct calculation of the inverse Hessian matrix required for minimization path retrieval and therefore proved most efficient. Analytical first partial derivatives $\partial J_i/\partial P_j$ of the coupling constant J_i with respect to each of the fit parameters P_j were provided to accelerate the mixed quadratic and cubic line search algorithm. However, search direction update in the course of gradient evaluation, i.e. Hessian matrix recomputation, turned out to be the time-limiting step. At 64 bit floating-point representation, benchmarks on an Intel 486/50-based personal computer required ca. 4 and 23 CPU seconds per gradient step for 140 and 252 fit parameters in the flavodoxin application, respectively. Typically, the procedure converged after a few cycles of 400 function and 100 gradient evaluations, between which each torsion-angle value was swept through the complete 2π interval while evaluating its contribution to ϵ_J^2 in order to escape from local minima due to possible degenerate solutions.

Gradient computation at arbitrary points in the multi-dimensional model space involves derivatives with respect to Fourier coefficients, $\partial J/\partial C_m = \cos(m\theta)$, to torsion angles, $\partial J/\partial\theta = -\{C_1\sin(\theta) + 2C_2\sin(2\theta)\}$, and to distribution width parameters, $\partial J/\partial\sigma_\theta = -\sigma_\theta\{C_1\exp(-\sigma_\theta^2/2)\cos(\theta) + 4C_2\exp(-2\sigma_\theta^2)\cos(2\theta)\}$. The partial derivative of the fit error with respect to any of the variables was constructed from a merger of Equation 4 and one of the above mentioned functions according to $\partial\epsilon_J^2/\partial P_j = \partial\epsilon_J^2/\partial J_i \cdot \partial J_i/\partial P_j = 2\sum_i^n \sigma_i^{-2}\Delta J_i \cdot \partial J_i/\partial P_j$ where ΔJ is the current deviation from the target coupling constant.

Results and discussion

Basic self-consistent J *coupling analysis in flavodoxin*

Accurate backbone ϕ torsion angles in the protein *D. vulgaris* flavodoxin were determined on the exclusive basis of J coupling constants related to all six possible pairs of scalar coupled nuclei. Transformation of the spin-system properties into dihedral angle parameters was achieved by a novel procedure, termed self-consistent evaluation of J coupling constants, the main feature of which is to take advantage of redundant structure information embedded in related J coupling data sets. At the same time, iterative numerical optimization delivered sets of Karplus coefficients, which are considered empirical descriptors of the dihedral angle dependence of J values. Optimized Karplus coefficients and torsion angle geometries are summarized in Table 1 and Table 2, respectively. The global rms deviation between calculated and experimental coupling constants was 0.35 Hz which reflects the gross experimental precision of J coupling determination. Individual rmsd values ranged from 0.25 to 0.44 Hz, with violations of $^3J(\mathrm{H^N},\mathrm{H^\alpha})$ coupling constants being smallest (Figure 3).

The refined Karplus coefficients given in Table 1 can be compared to recent X-ray coordinate-based parametrizations of the ϕ torsional dependences of all six possible couplings $^3J(\mathrm{H^N},\mathrm{H^\alpha})$, $^3J(\mathrm{H^N},\mathrm{C'})$, $^3J(\mathrm{H^N},\mathrm{C^\beta})$, $^3J(\mathrm{C'_{i-1}},\mathrm{H_i^\alpha})$, $^3J(\mathrm{C'_{i-1}},\mathrm{C'_i})$, and $^3J(\mathrm{C'_{i-1}},\mathrm{C_i^\beta})$ as derived by Bax and co-workers (Wang and

Table 2. Optimized ϕ torsion angles in flavodoxin as inferred from self-consistent *J* coupling analysis[a]

Residue	ϕ_{X-ray}	ϕ_{Rigid}	ϕ_{Gauss}	Residue	ϕ_{X-ray}	ϕ_{Rigid}	ϕ_{Gauss}	Residue	ϕ_{X-ray}	ϕ_{Rigid}	ϕ_{Gauss}
Lys-3	−107.0	−112.2	−112.4 ± 5.0	Leu-52	−141.4	−152.0	−148.6 ± 29.9	Phe-101	−63.5	−62.3	−60.3 ± 5.0
Ala-4	−120.3	−120.4	−121.5 ± 9.8	Val-53	−123.2	−117.8	−119.4 ± 14.8	Cys-102	53.0	49.9	38.4 ± 28.2
Leu-5	−113.5	−112.6	−117.8 ± 21.0	Leu-54	−113.3	−117.6	−118.3 ± 3.2	Ala-104	−61.3	−75.2	−74.0 ± 0.2
Ile-6	−119.2	−127.9	−129.7 ± 0.1	Leu-55	−112.2	−110.7	(n.a.)	Val-105	−61.4	−69.9	−68.5 ± 0.1
Val-7	−119.8	−119.5	−120.5 ± 10.3	Cys-57	−159.0	−153.9	−153.7 ± 17.0	Asp-106	−60.4	−63.7	−59.8 ± 19.5
Tyr-8	−131.5	−125.8	−127.6 ± 0.1	Ser-58	−85.4	−88.8	−87.9 ± 0.1	Ala-107	−64.3	−60.1	−58.1 ± 0.1
Ser-10	−142.2	−140.5	−140.8 ± 11.5	Thr-59	−109.2	−109.1	−108.0 ± 0.3	Ile-108	−67.3	−78.8	−78.4 ± 15.8
Thr-11	−93.3	−97.4	−96.3 ± 0.1	Trp-60	−125.4	−130.2	−131.7 ± 0.0	Glu-109	−59.5	−61.7	−58.3 ± 14.6
Thr-12	−106.0	−109.1	−108.7 ± 1.7	Asp-62	65.6	71.8	78.8 ± 39.8	Glu-110	−58.3	−62.9	−58.7 ± 19.3
Asn-14	−70.6	−70.8	−69.4 ± 10.4	Ser-64	−150.6	−155.2	−154.8 ± 18.7	Lys-111	−62.0	−74.1	−72.8 ± 15.5
Glu-16	−67.9	−75.5	−74.4 ± 12.4	Ile-65	−91.3	−86.0	−90.5 ± 29.6	Leu-112	−60.8	−64.0	−59.9 ± 0.0
Tyr-17	−60.5	−62.5	−59.5 ± 13.8	Glu-66	−120.0	−129.5	−131.2 ± 0.1	Lys-113	−64.3	−66.5	−62.7 ± 22.0
Ala-19	−59.2	−66.1	−64.4 ± 8.8	Leu-67	−79.4	−76.6	−75.5 ± 0.1	Asn-114	−73.5	−70.0	−67.3 ± 21.5
Glu-20	−68.7	−66.8	−62.8 ± 23.3	Gln-68	−49.4	−60.2	−57.7 ± 7.6	Leu-115	−78.7	−92.0	−92.8 ± 14.1
Thr-21	−65.7	−71.9	−70.3 ± 16.9	Asp-69	−50.8	−53.5	(n.a.)	Ala-117	−67.5	−79.0	−78.3 ± 11.2
Ile-22	−61.5	−71.9	−70.7 ± 8.0	Asp-70	−69.9	−78.2	−77.2 ± 0.1	Glu-118	−104.1	−93.0	−98.0 ± 24.4
Ala-23	−56.3	−59.9	−54.2 ± 20.3	Phe-71	−84.4	−86.2	−86.4 ± 14.0	Ile-119	−81.9	−83.3	−84.8 ± 23.6
Arg-24	−64.2	−68.9	−66.1 ± 21.0	Ile-72	−47.9	−56.1	−52.1 ± 11.8	Val-120	−78.7	−78.3	−78.3 ± 26.3
Glu-25	−65.3	(n.a.)	(n.a.)	Leu-74	−62.0	−79.7	−79.1 ± 13.0	Gln-121	−150.3	−158.3	−159.2 ± 0.1
Leu-26	−67.2	−74.9	−73.7 ± 25.3	Phe-75	−57.8	−66.0	−64.3 ± 6.8	Asp-122	−64.2	−67.4	−64.0 ± 22.5
Ala-27	−65.8	−65.7	−62.4 ± 18.1	Asp-76	−68.2	−65.1	−61.7 ± 18.4	Leu-124	−85.0	−93.1	−92.3 ± 0.1
Asp-28	−66.4	−70.1	−66.4 ± 26.7	Ser-77	−103.0	−112.9	(n.a.)	Arg-125	−114.1	−112.6	(n.a.)
Ala-29	−82.2	−94.2	−97.1 ± 19.4	Leu-78	−59.1	−44.6	−36.6 ± 12.4	Ile-126	−94.1	−101.1	−100.1 ± 0.1
Tyr-31	−71.1	−85.4	−84.5 ± 6.2	Glu-79	−59.5	−61.2	−55.7 ± 20.8	Asp-127	−96.6	−102.7	−104.0 ± 13.0
Glu-32	−94.3	−98.4	−97.6 ± 0.4	Glu-80	−96.8	−89.8	−90.4 ± 14.5	Asp-129	−63.4	−67.3	−65.0 ± 14.6
Val-33	−116.2	−114.4	−116.5 ± 15.0	Thr-81	−78.9	−78.8	−79.0 ± 26.2	Arg-131	−63.0	−76.3	−76.0 ± 25.5
Asp-34	−118.3	−117.8	−119.3 ± 15.1	Ala-83	−82.1	−79.2	−79.4 ± 24.5	Ala-132	−91.1	−92.3	−91.9 ± 8.6
Ser-35	−107.2	−113.1	−114.8 ± 13.6	Gln-84	−56.8	−63.1	−61.3 ± 0.6	Ala-133	−126.7	−115.7	−117.6 ± 14.6
Arg-36	−128.6	−131.9	−132.6 ± 10.2	Arg-86	−79.1	−86.8	−86.8 ± 12.9	Arg-134	−53.1	−42.3	−36.0 ± 0.1
Asp-37	−67.4	−83.1	−82.2 ± 0.1	Lys-87	−82.9	−85.1	−84.7 ± 9.3	Asp-135	−64.8	−68.2	−65.5 ± 19.5
Ala-38	−61.4	−59.2	−55.1 ± 15.4	Val-88	−133.4	−127.2	−129.0 ± 0.1	Asp-136	−68.7	−78.7	−78.2 ± 15.7
Ala-39	−58.4	−67.3	−66.0 ± 0.1	Ala-89	−153.1	−158.5	−159.4 ± 0.0	Ile-137	−68.9	−74.7	−73.6 ± 18.2
Ser-40	−94.5	−105.3	−107.2 ± 13.9	Cys-90	−120.6	−114.6	−114.7 ± 0.1	Val-138	−59.7	−67.5	−65.3 ± 14.7
Val-41	−112.1	−104.5	−107.0 ± 15.5	Phe-91	−147.7	−143.0	−144.5 ± 0.1	Trp-140	−66.7	−69.7	−67.9 ± 15.3
Glu-42	−110.5	−108.1	−114.8 ± 21.9	Cys-93	−105.1	−108.4	−107.6 ± 0.0	Ala-141	−61.3	−67.8	−65.1 ± 18.1
Ala-43	−64.4	−64.2	−61.1 ± 15.9	Asp-95	−149.3	−145.2	−145.9 ± 9.4	His-142	−63.6	−70.2	−68.3 ± 15.7
Leu-46	−49.9	−51.9	−40.6 ± 22.4	Ser-96	−65.5	−73.2	−70.7 ± 27.0	Asp-143	−63.4	−74.1	−72.9 ± 14.9
Phe-47	−86.7	−86.0	−85.9 ± 12.7	Ser-97	−76.4	−86.1	(n.a.)	Val-144	−63.9	−69.8	−67.0 ± 22.3
Glu-48	−61.2	−65.9	−62.3 ± 19.8	Tyr-98	−88.3	−98.0	−97.0 ± 0.1	Arg-145	−62.5	−77.6	−77.6 ± 27.2
Phe-50	−106.8	−101.8	−102.6 ± 11.8	Glu-99	−65.2	−68.3	−61.9 ± 32.0	Ala-147	−98.0	−89.8	−93.0 ± 22.5
Asp-51	−88.3	−87.6	−86.5 ± 0.0	Tyr-100	−105.9	−97.2	−106.3 ± 27.4	Ile-148	−113.2	−105.6	−110.1 ± 19.2

[a]Values ϕ_{Rigid} and ϕ_{Gauss} (in degrees) denote best fitting torsion angles as obtained in contexts of a rigid and a Gaussian-libration molecular model, respectively. (n.a.) not sufficient *J*-coupling constants available. $\phi_{X\text{-}ray}$ are crystallographic results as taken from Walsh (private communication).

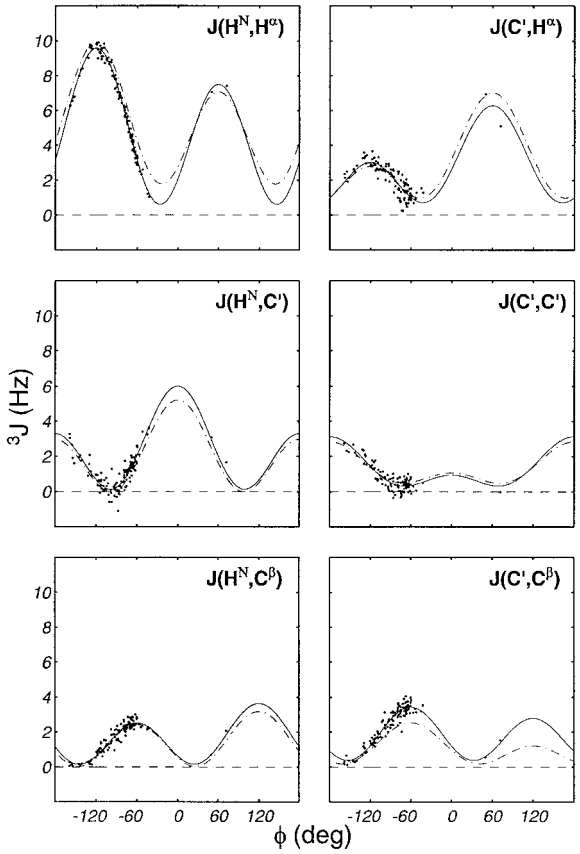

Figure 3. Self-consistent angular dependence of polypeptide ϕ-related ^3J-coupling constants. The optimized Karplus curves (solid lines) are compared with recent parameterizations (dot-dashed lines) of $^3J(H^N,H^\alpha)$, $^3J(H^N,C')$, $^3J(H^N,C^\beta)$, and $^3J(C'_{i-1}, H_i^\alpha)$ by Wang and Bax (1996), and of $^3J(C'_{i-1},C'_i)$ and $^3J(C'_{i-1},C_i^\beta)$ by Hu and Bax (1996, 1997). The comparatively reduced scatter in violations of $^3J(H^N,H^\alpha)$ coupling constants is rationalized by two facts: firstly, $^3J_{HH}$ values are larger than those of $^3J_{HC}$ or $^3J_{CC}$ on an absolute scale, and secondly, ϕ torsions in protein regular structure typically cover the markedly steep slope of the $^3J_{HH}$ curve, thus making the fit very sensitive to small changes in the intermediate values of $^3J_{HH}$.

Bax, 1995, 1996; Hu and Bax, 1996, 1997, 1998). As pointed out elsewhere (Blümel et al., 1998), the difference in either two sets of Karplus coefficients quantifies an average discrepancy in the (calculated) *J* coupling constants to be expected upon complete dihedral angle revolution through the 2π interval, as given by $\Delta J_{rms} = \{0.375(\Delta A)^2 + 0.5(\Delta B)^2 + (\Delta C)^2 + \Delta A \Delta C\}^{1/2}$. Accordingly, rms deviations between the reference curves and ours amount to 0.78, 0.43, 0.25, 0.48, 0.16, and 0.83 Hz, respectively, significantly exceeding experimental sensitivity. As shown in Figure 3 all of the Karplus curves differ most for conformations involving positive torsion angles, a fact attributed to sparse experimental sampling.

Comments are due on the intraresidual coupling constant $^3J(C',C^\beta)$ for which divergent Karplus parametrizations exist. Two attempts by Hu and Bax (1997, 1998) led to coefficients that, make *J* values topping at ca. 2.7 Hz, reflecting their experimental ubiquitin data. These parameter sets disagree with our parametrization by $\Delta J_{rms} = 0.83$ Hz and $\Delta J_{rms} = 1.08$ Hz, respectively. However, our experimental $^3J(C',C^\beta)$ values in flavodoxin are as large as 4.06 Hz. Löhr et al. (1997) reported significantly different $^3J(C',C^\beta)$ coefficients for which better agreement with the current work is obtained, $\Delta J_{rms} = 0.21$ Hz, obviously because the same sample protein and experimental methods have been used.

The ϕ torsional angles in *D. vulgaris* flavodoxin as derived from *J* coupling constants were compared with reference ϕ values from X-ray diffraction studies (Table 2). Figure 4 reveals strikingly similar conformations in both solution and solid state, which was not anticipated a priori. Half of the torsions (60 out of 122) agreed to within 5°, another 41 residues exhibited deviations between 5° and 10°, while only 21 torsions exceeded 10° deviation with the maximum at 17.7° for Leu-74.

ϕ-*torsion-angle dynamics in flavodoxin as inferred from* J *coupling information*

So far, *J* coupling analysis was based on the possibly unjustified assumption of a single rigid molecular conformation. Local intramolecular mobility and reorientation processes make *J* coupling constants dynamically averaged parameters (Jardetzki, 1980), so derivation of angular constraints becomes ambiguous. Due interpretation of experimental data then requires conformational flexibility be accounted for in the model. Rapid angular interconversion averages the experimental *J* coupling constant of (distinct) dihedral-angle states θ weighted by individual probabilities, i.e. $\langle J \rangle = \int_0^{2\pi} p(\theta) J(\theta) d\theta$. The dihedral-angle distribution profile $p(\theta)$ was considered to obey a simple Gaussian normal distribution (Karimi-Nejad et al., 1994; Schmidt, 1997b). With respect to both transparent implementation and computational speed, the convolution integral was approximated in terms of appropriately modified Karplus coefficients (Bruschweiler and Case, 1994).

Self-consistent calibration of Karplus coefficients, mean torsion angles, and Gaussian fluctuation widths

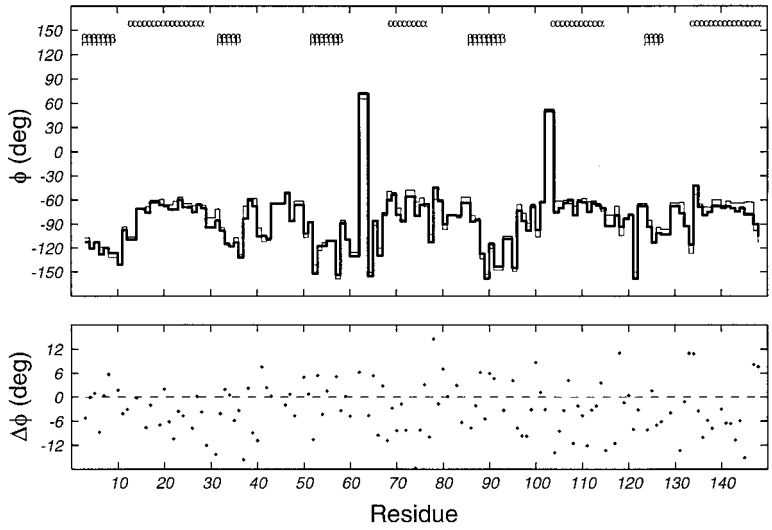

Figure 4. Torsion angles in flavodoxin as obtained from self-consistent *J* coupling analysis. In the upper panel, NMR-derived torsions (heavy line) are superimposed on reference values from high-resolution X-ray coordinates (light line). The lower panel shows (five-fold enlarged) the differences $\phi_{\text{NMR}} - \phi_{\text{X-ray}}$, the mean deviation and rms difference being $-2.9°$ and 7.0°, respectively. A secondary-structure-depending deviation is not perceived.

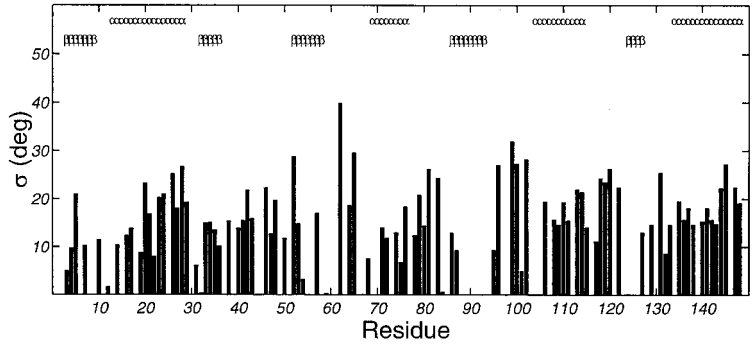

Figure 5. Amplitudes of Gaussian random fluctuation in the backbone of flavodoxin as inferred from ^3J coupling information. Secondary-structure elements α-helices and β-sheets are indicated by the respective symbols. Fluctuations in β-strands turned out to be smaller than in α-helical regions. The FMN-binding loops exhibit larger mobility.

revealed significant molecular mobility being present along the flavodoxin main chain. Mean torsions of both the rigid and the flexible model are found to agree within 3.3° on average. Figure 5 correlates mobility effects with secondary structure in the protein. In flavodoxin, residues 3–9, 32–36, 52–58, 86–93 and 124–127 are involved in β-sheet structures, while residues 13–28, 69–76, 104–114 and 134–148 participate in α-helix conformations. On average, ϕ-angular fluctuation turned out to be ±13.0° with α-helices appearing to be more flexible (±14.8°) than β-sheets (±7.7°). In flavodoxin, two loop regions (59–68 and 94–103) make up the FMN binding site which is ill-defined in the NOE-based NMR structure due to insufficient NOE distance information (Knauf et al., 1993, 1996). The lack of observable intraprotein NOE cross peaks for the respective residues is likely to be a consequence of the bound FMN molecule and/or local internal mobility. In fact, rigorous evaluation of local *J*-coupling information delivered conformational restraints on the accessible dihedral angle space, and at the same time hinted at comparatively large mobility of backbone torsions in the FMN binding loops (Table 2).

Global distortion from ideal bonding geometry

The dependence of the *J* coupling constants on bond-angle geometry was studied within the framework of rigid conformation. The prerequisite for associ-

ating distorted bond angles at N and C^{α} sites with a single global parameter each is met in so far as their first-sphere substituent pattern is identical in all amino acid types treated, except glycine and proline which were anyway excluded from the analysis. In a first trial, bending of the bond angle C'–C^{α}–C^{β} was parsed to the dihedral angles θ by adding increments ϑ as defined by Figure 1 and Table 1. The results showed only marginal deviation from tetrahedral geometry at the C^{α} atom. The optimized value of $\vartheta = -1.91 \pm 2.83°$ agrees well with the mean torsion difference $2\vartheta = \langle\theta(C'_{i-1}\text{–N–}C^{\alpha}\text{–}\ C_i^{\beta}) - \theta(C'_{i-1}\text{–N–}C^{\alpha}\text{–}C'_i) + 120°\rangle$ in the X-ray conformations grand averages of which amount to $-2.45 \pm 5.63°$ (2FX2, Watt et al., 1991) and $-0.69 \pm 3.93°$ (Walsh, unpublished). Similarly, amide nitrogen out-of-plane bending converged at $\xi = 3.82 \pm 3.02°$. However, comparison with X-ray data is impossible here due to the lack of hydrogen coordinates. Activating both fit parameters simultaneously revealed an even smaller bending tendency resulting in $\vartheta = -0.97 \pm 2.75°$ and $\xi = 3.44 \pm 3.02°$. Our data agree with the results of a recent investigation by Hu and Bax (1997) differing in both the method applied and the molecule studied. In conclusion, the assumption of perfect planar and tetrahedral geometry at N and C^{α} sites is justified.

Cross-validation and robustness of the method

Redundant data sets qualify for consistency tests using the procedure of cross-validation (Stone, 1974). The experimental set is partitioned at random into S distinct segments and processing using data from $S - 1$ segments is repeated for each of the S possible choices for the segment being omitted from the calculation. Values of the error function are collected separately for the included data as well as for the remaining segment and both test errors averaged over all S results. Data consistency is indicated when the combined residual does not significantly exceed the minimum error returned by the full target function, referred to as $\epsilon_J^2 = 1284.2$. Three cross-validation tests were carried out with partitioning (segment $\times$ element numbers) of 141×5, 47×15, and 15×47. The former two showed very good consistency with averaged summed residuals of 1303.0 and 1356.3, respectively. Karplus coefficients were within ± 0.06 and ± 0.14 Hz of the optimum solution (Table 1), respectively, while rms deviations between reference and cross-validated torsion angles were only 0.4° and 1.1°. Segment size was found too large in the third run, as about half a J-coupling information unit per residues was removed from the set. The summed residual and discrepancies in the Karplus coefficients and torsion angles leapt to 1812.4, ± 1.39 Hz, and 23.2°, respectively. Although results might vary with random segmentation, they efficiently demonstrate both the extent and utilization of redundance being present among the experimental observables.

An alternative way of partitioning has been adopted by Hu and Bax (1997) when keeping aside one out of six coupling constant types and predicting the omitted values, however, requiring Karplus coefficients for the latter be known. Such non-random partitioning is hardly applicable in our study because Karplus coefficients and torsion angles are iterated jointly. Trial analyses based on sets of only five J-coupling types, leaving out in turn each single column of the J matrix, worked fine in the flavodoxin case only if C^{β}-related coupling constants were omitted, but were found to depend on parameter initialization otherwise. Not surprisingly, unambiguous torsion angle determination indeed requires the maximum number of J-coupling types (Blümel et al., 1998). In contrast, stripping complete rows off the J matrix is readily tolerated, while computations are made on a smaller number of residues, eventually reverting all the advantage gained by imposing the concept of self consistently treating all available data.

By their very nature, ^3J-coupling constants, in particular heteronuclear ones, are confined to a narrow range of values and it is usually not possible to spot experimental outliers unless dealing with severely corrupted spectrum peaks. In a way, the robustness of our method is demonstrated by discerning those experimental J values which violate the back-calculated J values by more than three standard deviations, i.e. 0.75 Hz, as marked by triple asterisks in the supplementary Table S1 (to be obtained from the authors). In the set of 705 experimental values, there are 22 such violations accounting for 25% of the squared residual ϵ_J^2 but obviously they had no adverse effects on the torsion angle results.

Conclusions

In the context of NMR structure analysis, self consistency entails the joint interpretation of all structure information available for the majority of the macromolecular subunits, for example all amino acid residues in a protein. The concept involves simultaneous least-

squares optimization of a series of model parameters persistent to all residues while abandoning a priori assumptions on molecular properties usually inferred from either X-ray crystallography or other spectroscopic methods. By exploiting the data redundancy the entirety of the ϕ-related ^3J-coupling constants inheres, self consistent *J*-coupling evaluation applied to recombinant *Desulfovibrio vulgaris* flavodoxin was shown to deliver both accurate local ϕ torsion angles as well as reliable Karplus-type parameterization of the angular dependence of the spin-spin couplings referred. Final results showed not to depend on the actual starting geometry used, thus demonstrating the self-consistency of the procedure. As long as a fundamental theory of predicting *J*-coupling constants from molecular conformation is lacking, the calibration method outlined is expected to profit from the rapidly increasing amounts of *J* data and is likely to help improving the molecular models emerging from high-resolution conformational NMR studies.

Acknowledgements

We thank Dr M. Knauf and Professor S. Mayhew for their help in the preparation of recombinant isotope-enriched flavodoxin. Dr M. Walsh is thanked for making available the X-ray coordinates resolved at 0.17 nm prior to publication. This work was supported by the Deutsche Forschungsgemeinschaft under grant Ru 145/11-2.

References

Bax, A., Vuister, G.W., Grzesiek, S., Delaglio, F., Wang, A.C., Tschudin, R. and Zhu, G. (1994) *Methods Enzymol.*, **239**, 79–105.

Biamonti, C., Rios, C.B., Lyons, B.A. and Montelione, G.T. (1994) *Adv. Biophys. Chem.*, **4**, 51–120.

Billeter, M., Neri, D., Otting, G., Qian, Y.Q. and Wüthrich, K. (1992) *J. Biomol. NMR*, **2**, 257–274.

Blackledge, M.J., Brüschweiler, R., Griesinger, C., Schmidt, J.M., Xu, P. and Ernst, R.R. (1993) *Biochemistry*, **32**, 10960–10974.

Blümel, M., Schmidt, J.M., Löhr, F. and Rüterjans, H. (1998) *Eur. Biophys. J.*, **27**, 321–334.

Brünger, A.T. and Karplus, M. (1991) *Acc. Chem. Res.*, **24**, 54.

Brünger, A.T., Adams, P.D., Clore, G.M., Gros, P., Grosse-Kunstleve, R.W., Jiang, J.-S., Kuszewski, J., Nilges, M., Pannu, N.S., Read, R.J., Rice, L.M., Simonson, T. and Warren, G.L. (1998) *Acta Crystallogr.*, **D54**, 905–921.

Brüschweiler, R. and Case, D.A. (1994) *J. Am. Chem. Soc.*, **116**, 11199–11200.

Bystrov, V.F. (1976) *Prog. NMR Spectrosc.*, **10**, 41–81.

Case, D.A., Dyson, H.J. and Wright, P.E. (1994) *Methods Enzymol.*, **239**, 392–416.

Curley, G.P., Carr, M.C., Mayhew, S.G. and Voordouw, G. (1991) *Eur. J. Biochem.*, **202**, 1091–1100.

Davidson, W.C. (1959) *A.E.C. Research and Development Report*, ANL-5990.

DeMarco, A., Llinás, M. and Wüthrich, K. (1978a) *Biopolymers*, **17**, 637–650.

DeMarco, A., Llinás, M. and Wüthrich, K. (1978b) *Biopolymers*, **17**, 2727–2742.

DeMarco, A. and Llinás, M. (1979) *Biochemistry*, **18**, 3846–3854.

Eberstadt, M., Gemmecker, G., Mierke, D.F. and Kessler, H. (1995) *Angew. Chem.*, **107**, 1813–1838; *Angew. Chem. Int. Ed. Engl.*, **34**, 1671–1695.

Fischman, A.J., Live, D.H., Wyssbrod, H.R., Agosta, W.C. and Cowburn, D. (1980) *J. Am. Chem. Soc.*, **102**, 2533–2539.

Fletcher, R. and Powell, M.J.D. (1963) *Comput. J.*, **6**, 163–168.

Ghisla, S. and Massey, V. (1989) *Eur. J. Biochem.*, **181**, 1–17.

Güntert, P., Braun, W. and Wüthrich, K. (1991) *J. Mol. Biol.*, **217**, 517–530.

Güntert, P., Mumenthaler, C. and Wüthrich, K. (1997) *J. Mol. Biol.*, **273**, 283–298.

Haasnoot, C.A.G., de Leeuw, F.A.A.M. and Altona, C. (1980) *Tetrahedron*, **36**, 2783–2792.

Haasnoot, C.A.G., de Leeuw, F.A.A.M., de Leeuw, H.P.M. and Altona, C. (1981) *Biopolymers*, **20**, 1211–1245.

Hoch, J.C., Dobson, C.M. and Karplus, M. (1985) *Biochemistry*, **24**, 3831–3841.

Hu, J.-S. and Bax, A. (1996) *J. Am. Chem. Soc.*, **118**, 8170–8171.

Hu, J.-S. and Bax, A. (1997) *J. Am. Chem. Soc.*, **119**, 6360–6368.

Hu, J.-S. and Bax, A. (1998) *J. Biomol. NMR*, **11**, 199–203.

IUPAC-IUB Commission on Biochemical Nomenclature (1970) *J. Mol. Biol.*, **52**, 1–17; *Biochemistry*, **9**, 3471–3479.

Jardetzky, O. (1980) *Biochim. Biophys. Acta*, **621**, 227–232.

Karimi-Nejad, Y., Schmidt, J.M., Rüterjans, H., Schwalbe, H. and Griesinger, C. (1994) *Biochemistry*, **33**, 5481–5492.

Karplus, M. (1963) *J. Am. Chem. Soc.*, **85**, 2870–2871.

Knauf, M.A., Löhr, F., Curley, G.P., O'Farrell, P., Mayhew, S.G., Muller, F. and Rüterjans, H. (1993) *Eur. J. Biochem.*, **213**, 167–184.

Knauf, M.A., Löhr, F., Blümel, M., Mayhews, S.G. and Rüterjans, H. (1996) *Eur. J. Biochem.*, **238**, 423–434.

Kuboniwa, H., Grzesiek, S., Delaglio, F. and Bax, A. (1994) *J. Biomol. NMR*, **4**, 871–878.

Löhr, F. and Rüterjans, H. (1995) *J. Biomol. NMR*, **5**, 25–36.

Löhr, F. (1996) Ph.D. Thesis, University of Frankfurt am Main, Germany.

Löhr, F., Blümel, M., Schmidt, J.M. and Rüterjans, H. (1997) *J. Biomol. NMR*, **10**, 107–118.

Löhr, F. and Rüterjans, H. (1999) *J. Biomol. NMR*, **13**, 263–274.

Ludvigsen, S., Andersen, K.V. and Poulsen, F.M. (1991) *J. Mol. Biol.*, **217**, 731–736.

Mayhew, S.G. and Ludwig, M.L. (1975) In *The Enzymes* (Ed., Boyer, P.D.), Vol. 12, 3rd ed., Academic Press, New York, NY, pp. 57–118.

Mayhew, S.G. and Tollin, G. (1992) In *Chemistry and Biochemistry of flavoenzymes* (Ed., Müller, F.), Vol. 3, 3rd ed., CRC Press, Boca Raton, FL, pp. 389–426.

Mierke, D.F. and Kessler, H. (1992) *Biopolymers*, **32**, 1277–1282.

Pardi, A., Billeter, M. and Wüthrich, K. (1984) *J. Mol. Biol.*, **180**, 741–751.

Roberts, G.C.K. (Ed.) (1993) *NMR of Macromolecules: A Practical Approach*, Oxford University Press, Oxford, U.K.

Schmidt, J.M., Ernst, R.R., Aimoto, S. and Kainosho, M. (1995) *J. Biomol. NMR*, **6**, 95–105.

Schmidt, J.M., Löhr, F. and Rüterjans, H. (1996) *J. Biomol. NMR*, **7**, 142–152.
Schmidt, J.M. (1997a) *J. Magn. Reson.*, **124**, 298–309.
Schmidt, J.M. (1997b) *J. Magn. Reson.*, **124**, 310–322.
Stone, M. (1974) *J. R. Stat. Soc.*, **B36**, 111–147.
van Gunsteren, W.F. and Berendsen, H.J.C. (1985) In *Molecular Dynamics and Protein Structure*, (Ed., Herman, J.), Polycrystal Book Service, Western Springs, IL, pp. 5–14.
Vuister, G.W. and Bax, A. (1993) *J Am. Chem. Soc.*, **115**, 7772–7777.
Wang, A.C. and Bax, A. (1995) *J. Am. Chem. Soc.*, **117**, 1810–1813.
Wang, A.C. and Bax, A. (1996) *J. Am. Chem. Soc.*, **118**, 2483–2494.
Watt, W., Tulinsky, A., Swenson, R.P. and Watenpaugh, K.D. (1991) *J. Mol. Biol.*, **218**, 195–208.
Wüthrich, K. (1986) *NMR of Proteins and Nucleic Acids*, John Wiley, New York, NY.